



Crystal structure, Hirshfeld surface analysis and computational study of 2-chloro-*N*-[4-(methylsulfanyl)phenyl]acetamide

Sittichok Mongkholkeaw,^a Apisit Songsasen,^a Tanwawan Duangthongyou,^a Kittipong Chainok,^b Songwut Suramitr,^c Worawat Wattanathana^d and Boontana Wannalarse^{a*}

Received 25 February 2020

Accepted 3 March 2020

Edited by O. Blacque, University of Zürich, Switzerland

Keywords: 4-methylthioaniline; chloroacetyl chloride; hydrogen bonds; π - π interactions; crystal structure.

CCDC reference: 1987798

Supporting information: this article has supporting information at journals.iucr.org/e

^aDepartment of Chemistry and Center of Excellence for Innovation in Chemistry, Faculty of Science, Kasetsart University, Bangkok, 10900, Thailand, ^bMaterials and Textile Technology, Faculty of Science and Technology, Thammasat University, Pathum Thani, 12120, Thailand, ^cDepartment of Chemistry, Faculty of Science, Kasetsart University, Bangkok, 10900, Thailand, and ^dDepartment of Materials Engineering, Faculty of Engineering, Kasetsart University Bangkok, 10900, Thailand. *Correspondence e-mail: fscibnw@ku.ac.th

In the title compound, C₉H₁₀ClNOS, the amide functional group -C(=O)NH- adopts a *trans* conformation with the four atoms nearly coplanar. This conformation promotes the formation of a C(4) hydrogen-bonded chain propagating along the [010] direction. The central part of the molecule, including the six-membered ring, the S and N atoms, is fairly planar (r.m.s. deviation of 0.014). The terminal methyl group and the C(=O)CH₂ group are slightly deviating out-of-plane while the terminal Cl atom is almost in-plane. Hirshfeld surface analysis of the title compound suggests that the most significant contacts in the crystal are H···H, H···Cl/Cl···H, H···C/C···H, H···O/O···H and H···S/S···H. π - π interactions between inversion-related molecules also contribute to the crystal packing. DFT calculations have been performed to optimize the structure of the title compound using the CAM-B3LYP functional and the 6-311 G(d,p) basis set. The theoretical absorption spectrum of the title compound was calculated using the TD-DFT method. The analysis of frontier orbitals revealed that the π - π^* electronic transition was the major contributor to the absorption peak in the electronic spectrum.

1. Chemical context

Methylthioanilines are a class of S- and N- heterocyclic compounds that are widely used in antimicrobial applications (Chatterjee *et al.*, 2012; Martin *et al.*, 2016; Das *et al.*, 2017; Cross *et al.*, 2018). Metal-methylthioaniline complexes have also been utilized in many applications including as homogeneous catalysts, organic semiconductors, antibacterial and antifungal drugs (Chen *et al.*, 2019; Kumar *et al.*, 2017; Mandal *et al.*, 2018; Wang *et al.*, 2009). In this research, we report the synthesis and the solid state structure of 2-chloro-*N*-[4-(methylsulfanyl)phenyl]acetamide, a methylthioaniline derivative. Hirshfeld surface analysis was used to investigate the interactions within the crystal structure and DFT calculations were performed to study the frontier molecular orbitals of the title compound and also its electronic properties.

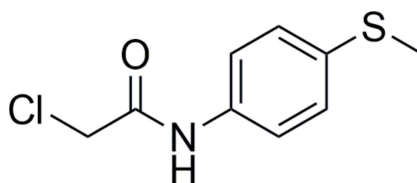
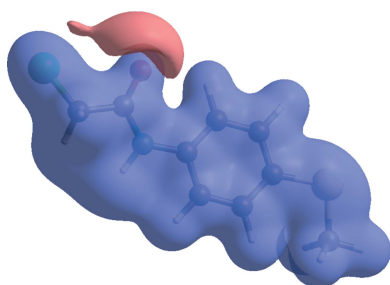


Table 1
 Hydrogen-bond geometry (Å, °).

$D-H\cdots A$	$D-H$	$H\cdots A$	$D\cdots A$	$D-H\cdots A$
$N1-H1\cdots O1^i$	0.82 (2)	2.06 (3)	2.875 (2)	174 (3)
$C1-H1B\cdots O1^i$	0.97	2.57	3.319 (3)	135
$C4-H4\cdots O1$	0.93	2.32	2.903 (3)	121

 Symmetry code: (i) $x + \frac{1}{2}, y, -z + \frac{3}{2}$.

2. Structural commentary

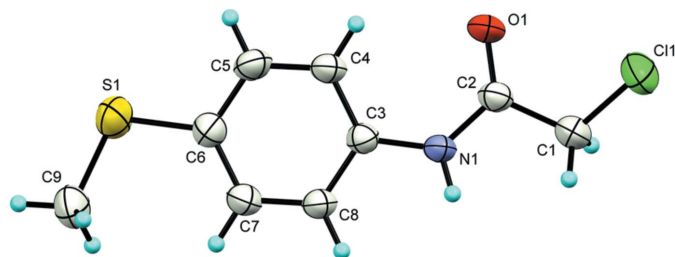
The asymmetric unit of the title compound contains one molecule (Fig. 1). The central part of the molecule, including the six-membered ring, the S and N atoms, is fairly planar (r.m.s. deviation of 0.0142 for the eight fitted non-hydrogen atoms). The terminal methyl group deviates from this plane, atom C9 being displaced by -0.498 (4) Å to the mean plane. On the other side of the benzene ring, the $C(=O)CH_2$ group also deviates slightly from the central plane in the opposite direction [deviations of 0.246 (3), 0.324 (3) and 0.489 (4) Å for atoms C2, O1 and C1, respectively] while the terminal Cl atom is almost in-plane [-0.007 (3) Å] as a result of the $N1-C2-C1-Cl1$ torsion angle of -150.97 (18)°. The amide functional group adopts a *trans* conformation with the four atoms nearly coplanar as shown by the $O1-C2-N1-H1$ torsion angle of -176.5 (19)°. An intramolecular $C-H\cdots O$ contact is observed (Table 1).

3. Supramolecular features

The main feature of the crystal packing is the presence of an $N-H\cdots O$ hydrogen-bonded chain along the *a*-axis direction (Table 1) with graph set $C(4)$. A view along the *a* axis showing the unit-cell packing is shown in Fig. 2*a* while the hydrogen-bonded chain is illustrated in Fig. 2*b*. Apart from the hydrogen-bonding interactions, π - π stacking is observed between inversion-related molecules. The distance between the ring centroids is 3.8890 (14) Å while the distance between the mean planes is 3.3922 (10) Å (slippage 1.904 Å).

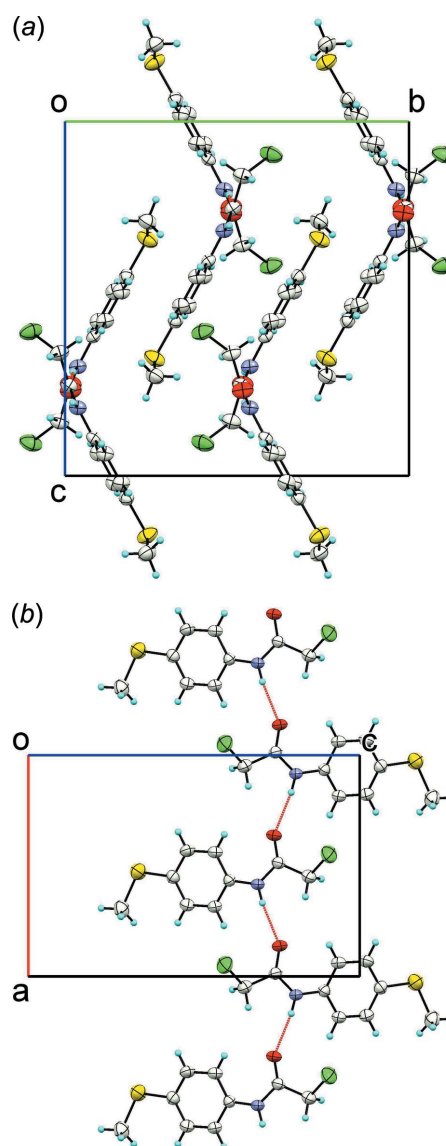
4. Hirshfeld analysis

The intermolecular interactions in the crystal of the title compound were investigated by performing a Hirshfeld


Figure 1

The molecular structure of the title compound, showing the atom-labelling scheme and displacement ellipsoids at the 50% probability level.

surface (HS) analysis (Hirshfeld, 1977; Spackman & Jayatilaka, 2009) using *Crystal Explorer 17.5* (Turner *et al.*, 2017). The HS is plotted over the d_{norm} range -0.5588 to 1.0138 a.u. (Fig. 3). The faint red spots on the Hirshfeld surface near atoms O1 and H1 confirm the hydrogen bonding described above. The presence of adjacent orange and blue triangular regions in the shape-index HS (Fig. 4) confirm that π - π interactions also occur in the crystal. Fig. 5 shows the full two-dimensional fingerprint plot (McKinnon *et al.*, 2007) and those delineated into $H\cdots H$ (35.5%), $H\cdots Cl/Cl\cdots H$ (19.2%), $H\cdots C/C\cdots H$ (11.8%), $H\cdots O/O\cdots H$ (11.6%) and $H\cdots S/S\cdots H$ (9.7%) contacts. The $H\cdots H$ contacts are characterized by a single spike at $d_e + d_i \simeq 2.2$ Å, while the $H\cdots O/O\cdots H$ contacts are viewed as a pair of spikes at $d_e + d_i \simeq 1.8$ Å. Two


Figure 2

The molecular packing in the title compound: (a) view of the unit-cell contents shown in projection down the *a* axis; (b) view of the supramolecular chain perpendicular to the *b* axis originated by the $N-H\cdots O$ hydrogen bonding (shown as red dashed lines). Displacement ellipsoids are drawn at the 50% probability level.

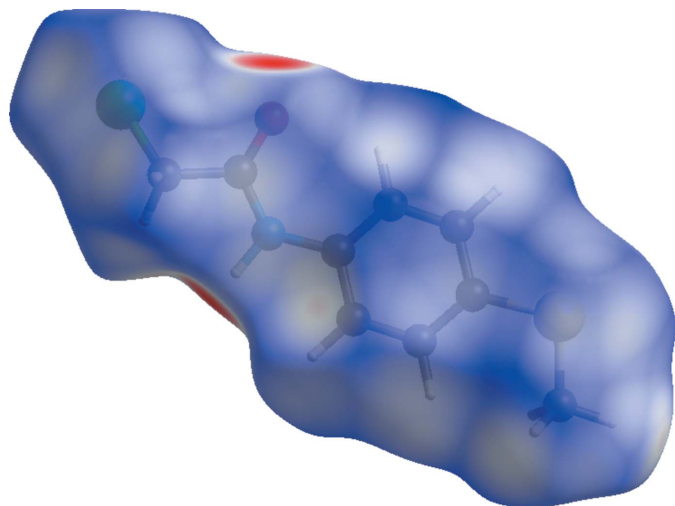


Figure 3
View of the three-dimensional Hirshfeld surface of the title compound plotted over d_{norm} in the range -0.5588 to 1.0138 a.u.

pairs of beak-shaped tips at $d_e + d_i \simeq 2.8$ and 3.1 Å represent $\text{H}\cdots\text{Cl}/\text{Cl}\cdots\text{H}$ and $\text{H}\cdots\text{S}/\text{S}\cdots\text{H}$ contacts, respectively. The $\text{H}\cdots\text{C}/\text{C}\cdots\text{H}$ contacts are seen as forcep-like tips at $d_e + d_i \simeq 2.7$ Å. Other contacts with smaller contributions to the HS have a less significant effect on the crystal packing: $\text{C}\cdots\text{Cl}/\text{Cl}\cdots\text{C}$ (2.9%), $\text{C}\cdots\text{S}/\text{S}\cdots\text{C}$ (2.1%), $\text{H}\cdots\text{N}/\text{N}\cdots\text{H}$ (2.1%) and $\text{C}\cdots\text{C}$ (2.8%).

5. Computational Methods

DFT calculations were carried out to optimize the structure of the title compound using the CAM-B3LYP method and the 6-311G(d,p) basis set in an ethanol solvent within the *Gaussian09* program package (Frisch *et al.*, 2010). DFT was chosen because it is a good compromise between the computational

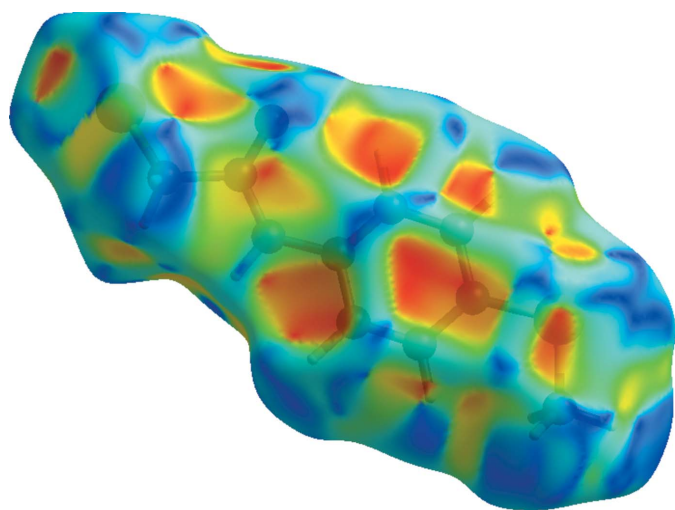


Figure 4
The shape-index Hirshfeld surface of the title compound plotted in the range from -1.0000 to 1.0000 a.u.

time and the description of the electronic correlation and has been found to be the best method to obtain accuracy for molecular geometry and electronic transition energies for organic molecules (Perdew *et al.*, 2005; Niskanen *et al.*, 2014; Ari *et al.*, 2017; Miengmern *et al.*, 2019). Time-dependent density functional theory (TD-DFT) (Jacquemin *et al.*, 2009) was also used for the calculation of the electronic transitions of the title compound in conjunction with the polarized continuum model (PCM) for computation of the solvent effect (Scalmani *et al.*, 2010). The theoretical absorption spectrum of the optimized structure of the titled compound in ethanol solvent was obtained using the TD-DFT method. The electronic properties such as E_{HOMO} , E_{LUMO} , and the energy gap between HOMO and LUMO of the optimized structure were also determined and the electronic structure of the title compound was visualized in order to understand the hyperconjugative interactions and charge delocalization.

6. Computational study

The DFT structure optimization of the compound was performed starting from the X-ray geometry at the CAM-B3LYP/6-311G(d,p) level of theory in an ethanol solvent. The experimental and calculated geometrical parameters such as bond lengths and angles show good agreement although most of the calculated bond lengths are slightly longer than X-ray values (about 0.01 Å) because experimental values are for interacting molecules in the crystal lattice, whereas the computational method deals with an isolated molecule in the solvent phase.

We used the TD-CAM-B3LYP/6-311G(d,p) method to predict the absorption spectrum of the title compound in ethanol, also considering the excited states in the calculation. The maximum absorption wavelength (λ_{max}) of the title compound was obtained using this method. As seen in Table 2,

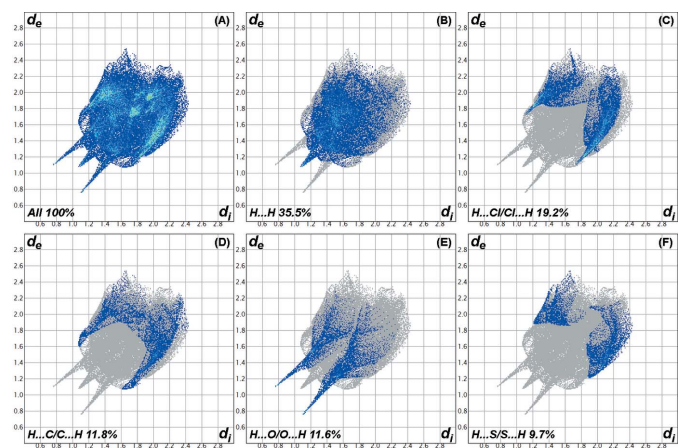


Figure 5
The full two-dimensional fingerprint plot for the title compound, showing (a) all interactions and those delineated into (b) $\text{H}\cdots\text{H}$, (c) $\text{H}\cdots\text{Cl}/\text{Cl}\cdots\text{H}$, (d) $\text{H}\cdots\text{C}/\text{C}\cdots\text{H}$, (e) $\text{H}\cdots\text{O}/\text{O}\cdots\text{H}$ and (f) $\text{H}\cdots\text{S}/\text{S}\cdots\text{H}$ interactions. The d_i and d_e values are the closest internal and external distances (in Å) from given points on the Hirshfeld surface.

Table 2

The electronic absorption spectrum of the title compound calculated by the TD-CAM-B3LYP/6-311G(d,p) method.

Excited states	Excitation energy			Configurations composition
	eV	nm	<i>f</i>	
$S_0 \rightarrow S_1$	4.80	258	0.0354	HOMO \rightarrow L+1 (84%)
$S_0 \rightarrow S_2$	4.95	250	0.7144	HOMO \rightarrow LUMO (91%)
$S_0 \rightarrow S_3$	5.55	224	0.0000	HOMO \rightarrow L+3 (81%)
$S_0 \rightarrow S_4$	5.63	220	0.0005	H-3 \rightarrow LUMO (69%)
$S_0 \rightarrow S_5$	6.35	195	0.1378	H-1 \rightarrow LUMO (59%)

the strong absorption at $\lambda_{\max} = 250$ nm and the oscillator strength $f = 0.7144$ are due to the $S_0 \rightarrow S_2$ electronic transition with a wave function of two configurations [(HOMO \rightarrow LUMO) and (HOMO \rightarrow L+4)]. The transition from HOMO to LUMO is mainly responsible for the formation of the maximum wavelength at 250 nm (Table 3). Fig. 6 shows the shape of molecular orbitals participating in the absorption at $\lambda_{\max} = 250$ nm. The electron density of the HOMO is mainly focused on the $-\text{C}=\text{C}-$ group in the phenyl ring, the sulfur atom, $\text{S}-\text{CH}_3$, $-\text{NH}=\text{C}$ and $-\text{C}=\text{O}$ groups, whereas the LUMO is mainly focused on the $=\text{C}-\text{C}=\text{C}$ group in the phenyl ring. Therefore, the electronic transition from HOMO to LUMO mainly corresponds to the $\pi-\pi^*$ electron. The other excited states of the title compound have a very small intensity that is nearly forbidden by orbital symmetry considerations.

7. Database survey

A search of the Cambridge Structural Database (CSD version 5.41, November 2019 update; Groom *et al.*, 2016) for the 2-chloro-*N*-phenylacetamide core shows that most of the structures were reported by Gowda and Co-workers, for example, the compound 2-chloro-*N*-phenylacetamide (I) (RIYWIG; Gowda *et al.*, 2008a) reported in the *Cc* space group. Other structures with substituent(s) on the benzene ring include 2-chloro-*N*-(2,3-dichlorophenyl)acetamide (II) (GISWEL; Gowda *et al.*, 2008b) in the $P2_1/n$ space group, 2-chloro-*N*-(3,5-dichlorophenyl)acetamide (III) (GISWIP;

Gowda *et al.*, 2008c) also in $P2_1/n$, and 2-chloro-*N*-(2,4-dimethylphenyl)acetamide (IV) (YIRJAL; Gowda *et al.*, 2008d) in $P\bar{1}$. The title compound and compounds (I)–(IV) crystallized in different space groups so it can be concluded that the substituent(s) play a vital role in the crystallization of 2-chloro-*N*-phenylacetamide derivatives. It is worth noting that the structures all of the above 2-chloro-*N*-phenylacetamide derivatives feature a *C*(4) hydrogen-bond chain involving the primary amide functional group. This feature was also observed in the crystal structures of 2,2-chloro-*N*-phenylacetamide derivatives, *viz.* 2,2-dichloro-*N*-(2,3-dimethylphenyl)acetamide (V) (space group *C2/c*; XISROH; Gowda *et al.*, 2008e) and 2,2-dichloro-*N*-(3,5-dimethylphenyl)acetamide (VI) ($P2_1/n$; GISGUL; Gowda *et al.*, 2008f) and the crystal structure of the derivative with no substituent on the 2nd position, [*N*-(3-chlorophenyl)acetamide] (VII) ($P2_12_12_1$; GISPOO; Gowda *et al.*, 2008g). This suggests that the substituents on both the benzene ring and at the 2-position did not affect the hydrogen-bonded framework in the *N*-phenylacetamide crystal structures. However, the derivatives with an *N,N*-disubstituted acetamide moiety cannot form hydrogen bonds in the same fashion as the *N*-monosubstituted acetamide derivatives because of the lack of a hydrogen-bond donor on the amide nitrogen atom. The supramolecular packing of *N,N*-disubstituted acetamide derivatives instead features weak intermolecular $\text{C}-\text{H} \cdots \text{O}$ interactions (Zhi *et al.*, 2011).

8. Synthesis and crystallization

The title compound was prepared by combining 4-(methylthio)aniline (5.0 g), chloroacetylchloride (4.30 mL) and triethylamine (7.50 mL) in dichloromethane (10 mL) at a controlled temperature using an ice bath. After stirring under an N_2 atmosphere for 24 h, the reaction mixture was poured into water and extracted with 30 mL CH_2Cl_2 (3 times). The organic layer was dried with anhydrous Na_2SO_4 . The mixture product was purified by column chromatography using 9:1 $\text{CH}_2\text{Cl}_2/\text{EtOAc}$ as an eluent, affording a light-brown solid, yield 42%. Light-brown crystals were grown by evaporating a solution of the title compound in a mixture of dichloromethane and hexane (1:1) at room temperature. ^1H NMR (CHCl_3 -*d*; 400 MHz): δ 8.23 (1H, *s*, NH), 7.51 (2H, *d*, ArH), 7.29 (2H, *d*, ArH), 4.20 (2H, *s*, CH_2), 2.50 (3H, *s*, SCH_3). Analysis calculated: $\text{C}_9\text{H}_{10}\text{ClNO}$: C, 50.11; H, 4.67; N, 6.49 Found: C, 50.44; H, 4.69; N, 6.50

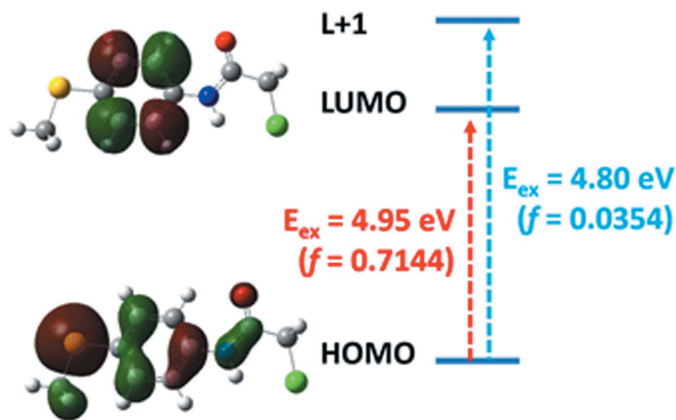


Figure 6

The molecular orbitals (MO) regarding information of the absorption spectrum of the title compound at the $S_0 \rightarrow S_1$ and $S_0 \rightarrow S_2$ states calculated by the CAM-B3LYP/6-311 G(d,p) method.

9. Refinement

Crystal data, data collection and structure refinement details are summarized in Table 3. All C-bound H atoms were positioned geometrically and refined using a riding model with $d(\text{C}-\text{H}) = 0.95 \text{ \AA}$ and $U_{\text{iso}}(\text{H}) = 1.2U_{\text{eq}}(\text{C})$ for aromatic and $d(\text{C}-\text{H}) = 0.98 \text{ \AA}$, $U_{\text{iso}}(\text{H}) = 1.5U_{\text{eq}}(\text{C})$ for methyl H atoms. The N-bound H atom (H1) was located in a difference-Fourier map and freely refined.

Acknowledgements

The authors thank the Kasetsart University Research and Development Institute, the Center of Excellence for Innovation in Chemistry (PERCH-CIC), the Ministry of Higher Education, Science, Research and Innovation, and the Department of Chemistry, Kasetsart University for financial support.

References

Arı, H. & Büyükmumcu, Z. (2017). *Comput. Mater. Sci.* **138**, 70–76.

Bruker (2016). *APEX2*, *SAINT* and *SADABS*. Bruker AXS Inc., Madison, Wisconsin, USA.

Chatterjee, S. K., Roy, S., Barman, S. K., Maji, R. C., Olmstead, M. M. & Patra, A. K. (2012). *Inorg. Chem.* **51**, 7625–7635.

Chen, S.-Q., Jiao, J.-Y., Zhang, X.-H. & Zhang, X. (2019). *Tetrahedron*, **75**, 246–252.

Cross, E. D., Ang, M. T. C., Richards, D. D., Clemens, A. D., Muthukumar, H., McDonald, R., Woodfolk, L., Ckless, K. & Bierenstiel, M. (2018). *Inorg. Chim. Acta*, **481**, 69–78.

Das, U. K., Daifuku, S. L., Iannuzzi, T. E., Gorelsky, S. I., Korobkov, I., Gabidullin, B., Neidig, M. L. & Baker, R. T. (2017). *Inorg. Chem.* **56**, 13766–13776.

Dolomanov, O. V., Bourhis, L. J., Gildea, R. J., Howard, J. A. K. & Puschmann, H. (2009). *J. Appl. Cryst.* **42**, 339–341.

Frisch, M. J., Trucks, G. W., Schlegel, H. B., Scuseria, G. E., Robb, M. A., Cheeseman, J. R., Scalmani, G., Barone, V., Mennucci, B., Petersson, G. A., Nakatsuji, H., Caricato, M., Li, X., Hratchian, H. P., Izmaylov, A. F., Bloino, J., Zheng, G., Sonnenberg, J. L., Hada, M., Ehara, M., Toyota, K., Fukuda, R., Hasegawa, J., Ishida, M., Nakajima, T., Honda, Y., Kitao, O., Nakai, H., Vreven, T., Montgomery, J. A. Jr, Peralta, J. E., Ogliaro, F., Bearpark, M., Heyd, J. J., Brothers, E., Kudin, K. N., Staroverov, V. N., Keith, T., Kobayashi, R., Normand, J., Raghavachari, K., Rendell, A., Burant, J. C., Iyengar, S. S., Tomasi, J., Cossi, M., Rega, N., Millam, J. M., Klene, M., Knox, J. E., Cross, J. B., Bakken, V., Adamo, C., Jaramillo, J., Gomperts, R., Stratmann, R. E., Yazyev, O., Austin, A. J., Cammi, R., Pomelli, C., Ochterski, J. W., Martin, R. L., Morokuma, K., Zakrzewski, V. G., Voth, G. A., Salvador, P., Dannenberg, J. J., Dapprich, S., Daniels, A. D., Farkas, O., Foresman, J. B., Ortiz, J. V., Cioslowski, J. & Fox, D. J. (2010). *Gaussian 09*, Revision B.01. Gaussian Inc, Wallingford CT, USA.

Gowda, B. T., Foro, S. & Fuess, H. (2008b). *Acta Cryst.* **E64**, o419.

Gowda, B. T., Foro, S. & Fuess, H. (2008c). *Acta Cryst.* **E64**, o420.

Gowda, B. T., Foro, S. & Fuess, H. (2008d). *Acta Cryst.* **E64**, o85.

Gowda, B. T., Foro, S. & Fuess, H. (2008g). *Acta Cryst.* **E64**, o381.

Gowda, B. T., Kožíšek, J., Tokarčík, M. & Fuess, H. (2008a). *Acta Cryst.* **E64**, o987.

Gowda, B. T., Svoboda, I., Foro, S., Paulus, H. & Fuess, H. (2008e). *Acta Cryst.* **E64**, o234.

Gowda, B. T., Svoboda, I., Foro, S., Paulus, H. & Fuess, H. (2008f). *Acta Cryst.* **E64**, o209.

Groom, C. R., Bruno, I. J., Lightfoot, M. P. & Ward, S. C. (2016). *Acta Cryst.* **B72**, 171–179.

Hirshfeld, F. L. (1977). *Theor. Chim. Acta*, **44**, 129–138.

Table 3

Experimental details.

Crystal data	
Chemical formula	C ₉ H ₁₀ CINOS
M_r	215.69
Crystal system, space group	Orthorhombic, <i>Pbca</i>
Temperature (K)	296
a, b, c (Å)	9.6659 (7), 14.0682 (11), 14.4869 (13)
V (Å ³)	1970.0 (3)
Z	8
Radiation type	Mo $K\alpha$
μ (mm ⁻¹)	0.56
Crystal size (mm)	0.12 × 0.10 × 0.08
Data collection	
Diffractometer	Bruker APEXII CCD
Absorption correction	Multi-scan (<i>SADABS</i> ; Bruker, 2016)
$T_{\text{min}}, T_{\text{max}}$	0.686, 0.746
No. of measured, independent and observed [$I > 2\sigma(I)$] reflections	21994, 2438, 1722
R_{int}	0.085
$(\sin \theta/\lambda)_{\text{max}}$ (Å ⁻¹)	0.667
Refinement	
$R[F^2 > 2\sigma(F^2)], wR(F^2), S$	0.047, 0.127, 1.02
No. of reflections	2438
No. of parameters	123
H-atom treatment	H atoms treated by a mixture of independent and constrained refinement
$\Delta\rho_{\text{max}}, \Delta\rho_{\text{min}}$ (e Å ⁻³)	0.51, -0.41

Computer programs: *APEX2* and *SAINT* (Bruker, 2016), *SHELXT2014/5* (Sheldrick, 2015a), *SHELXL2018/3* (Sheldrick, 2015b), *OLEX2* (Dolomanov *et al.*, 2009) and *Mercury* (Macrae *et al.*, 2020).

Jacquemin, D., Wathelet, V., Perpète, E. A. & Adamo, C. (2009). *J. Chem. Theory Comput.* **5**, 2420–2435.

Kumar, S. B., Solanki, A. & Kundu, S. (2017). *J. Mol. Struct.* **1143**, 163–167.

Macrae, C. F., Sovago, I., Cottrell, S. J., Galek, P. T. A., McCabe, P., Pidcock, E., Platings, M., Shields, G. P., Stevens, J. S., Towler, M. & Wood, P. A. (2020). *J. Appl. Cryst.* **53**, 226–235.

Mandal, S., Mondal, M., Biswas, J. K., Cordes, D. B., Slawin, A. M. Z., Butcher, R. J., Saha, M. & Chandra Saha, N. (2018). *J. Mol. Struct.* **1152**, 189–198.

Martin, D. J., McCarthy, B. D., Piro, N. A. & Dempsey, J. (2016). *Polyhedron*, **114**, 200–204.

McKinnon, J. J., Jayatilaka, D. & Spackman, M. A. (2007). *Chem. Commun.* 3814–3816.

Miengmern, N., Koonwong, A., Sriyab, S., Suramitr, A., Poo-arporn, R. P., Hannongbua, S. & Suramitr, S. (2019). *J. Lumin.* **210**, 493–500.

Niskanen, M. & Hukka, T. I. (2014). *Phys. Chem. Chem. Phys.* **16**, 13294–13305.

Perdew, J. P., Ruzsinszky, A., Tao, J., Staroverov, V. N., Scuseria, G. E. & Csonka, G. I. (2005). *J. Chem. Phys.* **123**, 1–9.

Scalmani, G. & Frisch, M. J. (2010). *J. Chem. Phys.* **132**, 114110–114115.

Sheldrick, G. M. (2015a). *Acta Cryst.* **A71**, 3–8.

Sheldrick, G. M. (2015b). *Acta Cryst.* **C71**, 3–8.

Spackman, M. A. & Jayatilaka, D. (2009). *CrystEngComm*, **11**, 19–32.

Turner, M. J., McKinnon, J. J., Wolff, S. K., Grimwood, D. J., Spackman, P. R., Jayatilaka, D. & Spackman, M. A. (2017). *Crystal Explorer 17*. The University of Western Australia.

Wang, Y., Tran, H. D. & Kaner, R. B. (2009). *J. Phys. Chem. C*, **113**, 10346–10349.

Zhi, L.-H., Wu, W.-N., Li, X.-X., Li, Y.-W. & Wang, Y. (2011). *Acta Cryst.* **E67**, o68.

supporting information

Acta Cryst. (2020). E76, 594-598 [https://doi.org/10.1107/S2056989020002960]

Crystal structure, Hirshfeld surface analysis and computational study of 2-chloro-*N*-[4-(methylsulfonyl)phenyl]acetamide

Sittichok Mongkolkeaw, Apisit Songsasen, Tanwawan Duangthongyou, Kittipong Chainok, Songwut Suramitr, Worawat Wattanathana and Boontana Wannalarse

Computing details

Data collection: *APEX2* (Bruker, 2016); cell refinement: *S SAINT* (Bruker, 2016); data reduction: *S SAINT* (Bruker, 2016); program(s) used to solve structure: *SHELXT2014/5* (Sheldrick, 2015a); program(s) used to refine structure: *SHELXL2018/3* (Sheldrick, 2015b); molecular graphics: *Olex2* (Dolomanov *et al.*, 2009) and *Mercury* (Macrae *et al.*, 2020); software used to prepare material for publication: *Olex2* (Dolomanov *et al.*, 2009) and *Mercury* (Macrae *et al.*, 2020).

2-Chloro-*N*-[4-(methylsulfonyl)phenyl]acetamide

Crystal data

C₉H₁₀ClNOS

$M_r = 215.69$

Orthorhombic, *Pbca*

$a = 9.6659$ (7) Å

$b = 14.0682$ (11) Å

$c = 14.4869$ (13) Å

$V = 1970.0$ (3) Å³

$Z = 8$

$F(000) = 896$

$D_x = 1.454$ Mg m⁻³

Mo $K\alpha$ radiation, $\lambda = 0.71073$ Å

Cell parameters from 3435 reflections

$\theta = 2.8$ – 26.2°

$\mu = 0.56$ mm⁻¹

$T = 296$ K

Block, light brown

$0.12 \times 0.10 \times 0.08$ mm

Data collection

Bruker APEXII CCD

diffractometer

φ and ω scans

Absorption correction: multi-scan

(SADABS; Bruker, 2016)

$T_{\min} = 0.686$, $T_{\max} = 0.746$

21994 measured reflections

2438 independent reflections

1722 reflections with $I > 2\sigma(I)$

$R_{\text{int}} = 0.085$

$\theta_{\max} = 28.3^\circ$, $\theta_{\min} = 2.8^\circ$

$h = -12 \rightarrow 12$

$k = -18 \rightarrow 17$

$l = -19 \rightarrow 17$

Refinement

Refinement on F^2

Least-squares matrix: full

$R[F^2 > 2\sigma(F^2)] = 0.047$

$wR(F^2) = 0.127$

$S = 1.02$

2438 reflections

123 parameters

0 restraints

Primary atom site location: dual

Hydrogen site location: mixed

H atoms treated by a mixture of independent and constrained refinement

$w = 1/[\sigma^2(F_o^2) + (0.051P)^2 + 1.0616P]$

where $P = (F_o^2 + 2F_c^2)/3$

$$(\Delta/\sigma)_{\max} < 0.001$$

$$\Delta\rho_{\max} = 0.51 \text{ e } \text{\AA}^{-3}$$

$$\Delta\rho_{\min} = -0.41 \text{ e } \text{\AA}^{-3}$$

Special details

Geometry. All esds (except the esd in the dihedral angle between two l.s. planes) are estimated using the full covariance matrix. The cell esds are taken into account individually in the estimation of esds in distances, angles and torsion angles; correlations between esds in cell parameters are only used when they are defined by crystal symmetry. An approximate (isotropic) treatment of cell esds is used for estimating esds involving l.s. planes.

Fractional atomic coordinates and isotropic or equivalent isotropic displacement parameters (\AA^2)

	<i>x</i>	<i>y</i>	<i>z</i>	$U_{\text{iso}}^*/U_{\text{eq}}$
Cl1	0.44778 (8)	0.40070 (6)	0.90711 (5)	0.0685 (3)
S1	0.52668 (8)	0.73979 (6)	0.33195 (5)	0.0612 (2)
O1	0.36226 (15)	0.51663 (13)	0.74128 (12)	0.0498 (4)
N1	0.58369 (17)	0.53698 (14)	0.69210 (13)	0.0364 (4)
H1	0.663 (3)	0.5277 (17)	0.7080 (18)	0.044*
C3	0.56559 (19)	0.58332 (15)	0.60636 (15)	0.0333 (4)
C7	0.6767 (2)	0.66353 (17)	0.47953 (16)	0.0423 (5)
H7	0.757186	0.685406	0.451533	0.051*
C2	0.4871 (2)	0.51212 (16)	0.75445 (16)	0.0370 (5)
C8	0.6844 (2)	0.61629 (17)	0.56270 (16)	0.0394 (5)
H8	0.770224	0.606313	0.590012	0.047*
C6	0.5498 (2)	0.67873 (16)	0.43719 (16)	0.0392 (5)
C4	0.4384 (2)	0.59718 (17)	0.56390 (17)	0.0404 (5)
H4	0.357922	0.574908	0.591632	0.048*
C5	0.4319 (2)	0.64410 (18)	0.48042 (17)	0.0440 (5)
H5	0.346335	0.652779	0.452346	0.053*
C1	0.5487 (2)	0.4838 (2)	0.84654 (17)	0.0477 (6)
H1A	0.559753	0.540211	0.884279	0.057*
H1B	0.639951	0.457030	0.836228	0.057*
C9	0.6958 (3)	0.7388 (2)	0.28174 (19)	0.0566 (7)
H9A	0.691402	0.764360	0.220355	0.085*
H9B	0.729678	0.674728	0.279361	0.085*
H9C	0.757047	0.776878	0.318558	0.085*

Atomic displacement parameters (\AA^2)

	U^{11}	U^{22}	U^{33}	U^{12}	U^{13}	U^{23}
Cl1	0.0643 (5)	0.0892 (6)	0.0520 (4)	−0.0232 (4)	0.0053 (3)	0.0168 (4)
S1	0.0566 (4)	0.0723 (5)	0.0548 (4)	0.0139 (3)	−0.0006 (3)	0.0206 (4)
O1	0.0241 (7)	0.0781 (12)	0.0471 (10)	−0.0002 (7)	0.0034 (6)	0.0045 (9)
N1	0.0227 (8)	0.0513 (11)	0.0353 (10)	−0.0003 (7)	0.0005 (7)	−0.0016 (8)
C3	0.0295 (9)	0.0378 (11)	0.0327 (11)	0.0009 (8)	−0.0001 (8)	−0.0055 (9)
C7	0.0332 (11)	0.0514 (14)	0.0423 (13)	−0.0058 (9)	0.0034 (9)	0.0001 (11)
C2	0.0279 (10)	0.0441 (12)	0.0389 (12)	−0.0001 (8)	0.0028 (8)	−0.0050 (10)
C8	0.0274 (10)	0.0517 (14)	0.0391 (12)	−0.0021 (9)	−0.0020 (8)	−0.0020 (10)
C6	0.0400 (12)	0.0391 (12)	0.0385 (12)	0.0028 (9)	−0.0003 (9)	−0.0021 (10)
C4	0.0266 (10)	0.0506 (13)	0.0440 (13)	−0.0006 (9)	0.0008 (9)	−0.0011 (10)

C5	0.0299 (10)	0.0548 (14)	0.0475 (14)	0.0058 (9)	-0.0057 (9)	-0.0015 (11)
C1	0.0348 (11)	0.0638 (16)	0.0444 (14)	-0.0040 (10)	0.0040 (10)	0.0069 (12)
C9	0.0628 (16)	0.0592 (17)	0.0478 (15)	-0.0048 (12)	0.0032 (12)	0.0110 (12)

Geometric parameters (Å, °)

Cl1—C1	1.757 (2)	C2—C1	1.515 (3)
S1—C6	1.764 (2)	C8—H8	0.9300
S1—C9	1.789 (3)	C6—C5	1.388 (3)
O1—C2	1.223 (2)	C4—H4	0.9300
N1—H1	0.82 (2)	C4—C5	1.379 (3)
N1—C3	1.414 (3)	C5—H5	0.9300
N1—C2	1.345 (3)	C1—H1A	0.9700
C3—C8	1.390 (3)	C1—H1B	0.9700
C3—C4	1.388 (3)	C9—H9A	0.9600
C7—H7	0.9300	C9—H9B	0.9600
C7—C8	1.378 (3)	C9—H9C	0.9600
C7—C6	1.388 (3)		
C6—S1—C9	103.42 (12)	C3—C4—H4	120.1
C3—N1—H1	116.1 (19)	C5—C4—C3	119.7 (2)
C2—N1—H1	115.1 (18)	C5—C4—H4	120.1
C2—N1—C3	128.60 (18)	C6—C5—H5	119.1
C8—C3—N1	116.83 (18)	C4—C5—C6	121.8 (2)
C4—C3—N1	124.31 (18)	C4—C5—H5	119.1
C4—C3—C8	118.9 (2)	Cl1—C1—H1A	108.9
C8—C7—H7	119.7	Cl1—C1—H1B	108.9
C8—C7—C6	120.6 (2)	C2—C1—Cl1	113.36 (16)
C6—C7—H7	119.7	C2—C1—H1A	108.9
O1—C2—N1	124.5 (2)	C2—C1—H1B	108.9
O1—C2—C1	122.62 (19)	H1A—C1—H1B	107.7
N1—C2—C1	112.76 (18)	S1—C9—H9A	109.5
C3—C8—H8	119.5	S1—C9—H9B	109.5
C7—C8—C3	120.9 (2)	S1—C9—H9C	109.5
C7—C8—H8	119.5	H9A—C9—H9B	109.5
C7—C6—S1	124.67 (18)	H9A—C9—H9C	109.5
C7—C6—C5	118.1 (2)	H9B—C9—H9C	109.5
C5—C6—S1	117.19 (17)		
S1—C6—C5—C4	-178.58 (19)	C2—N1—C3—C8	168.6 (2)
O1—C2—C1—Cl1	32.9 (3)	C2—N1—C3—C4	-11.7 (4)
N1—C3—C8—C7	-179.1 (2)	C8—C3—C4—C5	-0.8 (3)
N1—C3—C4—C5	179.4 (2)	C8—C7—C6—S1	178.92 (18)
N1—C2—C1—Cl1	-150.97 (18)	C8—C7—C6—C5	-0.7 (4)
C3—N1—C2—O1	8.9 (4)	C6—C7—C8—C3	-0.4 (4)
C3—N1—C2—C1	-167.2 (2)	C4—C3—C8—C7	1.2 (3)
C3—C4—C5—C6	-0.3 (4)	C9—S1—C6—C7	18.0 (2)
C7—C6—C5—C4	1.1 (4)	C9—S1—C6—C5	-162.3 (2)

Hydrogen-bond geometry (Å, °)

<i>D</i> —H \cdots <i>A</i>	<i>D</i> —H	H \cdots <i>A</i>	<i>D</i> \cdots <i>A</i>	<i>D</i> —H \cdots <i>A</i>
N1—H1 \cdots O1 ⁱ	0.82 (2)	2.06 (3)	2.875 (2)	174 (3)
C1—H1B \cdots O1 ⁱ	0.97	2.57	3.319 (3)	135
C4—H4 \cdots O1	0.93	2.32	2.903 (3)	121

Symmetry code: (i) $x+1/2, y, -z+3/2$.